JOURNAL OF GEOPHYSICAL RESEARCH, VOL. 106, NO. A3, PAGES 3655–3663, MARCH 1, 2001

Testing the thermospheric neutral wind suppression mechanism for day-to-day variability of equatorial spread *F*

Michael Mendillo

Center for Space Physics, Boston University, Boston, Massachusetts

John Meriwether

Department of Physics and Astronomy, Clemson University, Clemson, South Carolina

Manfred Biondi

Department of Physics and Astronomy, University of Pittsburgh, Pittsburgh, Pennsylvania

Abstract. The determination of the physical processes that cause the day-to-day variability of equatorial spread *F* (ESF) has long been one of the outstanding problems in terrestrial space physics. Within the context of the Rayleigh-Taylor instability model for ESF, mechanisms that either enhance or inhibit the growth of a seed perturbation offer potential sources of variability that can be tested. In this study the hypothesis that enhanced thermospheric meridional winds play a critical role in suppressing ESF is examined during the Multi-Instrumented Studies of Equatorial Thermospheric Aeronomy (MISETA) campaign of September 1998. New, high-time-resolution Fabry-Perot interferometer (FPI) observations at 6300-Å nightglow made at Arequipa (Peru) provided the neutral wind measurements during the critical postsunset hours that had been sampled only sparsely in earlier morphology studies. Evidence of local ESF activity was obtained using GPS-based observations of phase fluctuations (Fp) and 6300-Å all-sky optical images from the same site. Additional GPS measurements of Fp and total electron content (TEC) from Bogota (Colombia) and Santiago (Chile) were used to determine the full flux tube development of ESF plumes and to characterize the *F* region morphology of the interhemispheric Appleton anomaly. Correlative studies between the nightly magnitudes of the meridional winds (U_m), ESF activity (Fp), and indices describing the strength (I_s) and asymmetry (I_a) of the Appleton anomaly offered no convincing evidence for the wind suppression mechanism. The best available precursor for premidnight ESF appeared to be the strength of the electrodynamically driven Appleton anomaly pattern at sunset. If one assumes that the required seed perturbation for ESF onset is essentially always available, then for all practical purposes, the magnitude of the eastward electric field that causes upward drift is both the necessary and sufficient parameter to forecast ESF with reasonable success. These results reconfirm 60 years of study pointing to the dominance of electrodynamical processes in the onset and growth of plasma instabilities at low latitudes.

1. Introduction

Perhaps the most often described enigma in ionospheric physics is the seemingly capricious occurrence patterns of equatorial spread *F* (ESF). The many spatial and temporal scales of *F* region plasma irregularities that fall under the ESF designation were initially a source of confusion and controversy. In time, morphological classification schemes provided some real benefits in guiding physical explanations, and thus today the field is better off than, say, the magnetospheric community's attempt to agree upon what constitutes a substorm. The *F* region's classic "plasma bubble" encountered by a satellite sensor, the radar "backscatter plume," and the "airglow depletion" captured in an all-sky imager all refer to widely accepted views of an ESF event.

Paper number 2000JA000148.
0148-0227/01/2000JA000148$09.00

The statistical occurrence patterns of ESF are well known [*Aarons*, 1993], and a theoretical foundation based on the Rayleigh-Taylor gravitational instability mechanism [*Haerendel*, 1973; *Ossakow*, 1981; *Haerendel et al*., 1992] is both widely accepted and used successfully in computer simulations [*Zalesak et al*., 1982; *Maruyama and Matuura*, 1984; *Maruyama*, 1988; *Kuo et al*., 1998]. What remains to be understood is why, during the so-called "ESF season" at a given longitude, ESF does not occur every night. While it does occur on most nights, the reasons for its occasional absence have not been elucidated, presenting a challenge to our full understanding of this phenomenon. Moreover, from the application perspective that drives much of current space physics research, this aspect of forecasting ESF is of considerable importance.

The approach adopted for addressing the possible sources of day-to-day variability of the occurrence of ESF [e.g., *Mendillo et al*., 1992] has been to examine the physical processes described by various terms in the Rayleigh-Taylor growth rate (γ_{RT}) equation, as summarized by many authors (see reviews

by *Fejer* [1991, 1997], *Fuller-Rowell et al*. [1997], and *Kelley* [1989]):

$$\gamma_{\mathrm{RT}} = \left(\frac{\sum_P^F}{\sum_P^{E,N} + \sum_P^F + \sum_P^{E,S}} \right) \left[\frac{\vec{E} \times \vec{B}}{|B|^2} - \vec{U}_m - \frac{\vec{g}}{\nu_{in}} \right] \cdot \frac{\nabla N}{N}, \tag{1}$$

where all quantities (described below) are flux-tube-integrated parameters (see *Sultan* [1996a] and *Keskinen et al*. [1998] and references therein). Within this framework, ESF onset first requires a seed perturbation in electron density that appears where the plasma density altitude gradient is pronounced. Typically, such distortions of the ambient gradient are assumed to be generated via the propagation of a thermospheric gravity wave causing a few percent "ripple" in the steep, bottomside, postsunset electron density profile at altitudes from ~300 to 400 km [*Hysell et al*., 1990; *Huang and Kelley*, 1996]. Indeed, *McClure et al*. [1998] argue that the occurrence pattern for ESF depends primarily on the seasonal-longitudinal patterns of gravity waves produced by tropical convection events. Given such a seed perturbation, the main factor that then enhances γ_{RT} is a zonal electric field ($\vec{E}$) that raises the F layer to regions of low collision frequency (ν_{in}). Factors that can reduce γ_{RT} are a transequatorial neutral wind ($\vec{U}_m$) or the unusual appearance of a postsunset E layer that reduces the ratio of F region Pedersen conductivity (Σ_P^F) to the total flux tube conductivity ($\Sigma_P^{E,N} + \Sigma_P^F + \Sigma_P^{E,S}$) shown in (1). The impact of the meridional wind (U_m) upon the growth rate depends on its absolute magnitude ($|U_m|$), a consequence of the flux-tube-integrated physics, but a feature not apparent from the mathematical form of (1) (see *Sultan* [1996a] for a full discussion).

As reviewed recently by *Fejer et al*. [1999], it has long been proposed that the vertical plasma drift is the single most important factor in determining whether the Rayleigh-Taylor (R-T) instability occurs on a given night within the ESF season in a particular longitude sector. Yet for decades, there has been a widespread reluctance to accept the simple notion that a strong electrodynamical upward drift is both a necessary and sufficient condition for ESF onset and development. Given that situation, the variability issue metamorphosed into discussions of either a seed perturbation being absent or inhibiting mechanisms, on occasion, turning off a potential ESF event. *Mendillo et al*. [1992] discussed this situation at some length, suggesting that if seed perturbations are considered omnipresent, the variability issue reduces to identifying the operative inhibitor on a given night. They suggested that the meridional wind mechanism proposed by *Maruyama* [1988] for the explanation of seasonal-longitude-dependent ESF might also be invoked to explain day-to-day variability [*Zalesak and Huba*, 1991]. This paper deals with a test of that proposal.

The NSF-sponsored programs of Multi-Instrumented Studies of Equatorial Thermospheric Aeronomy (MISETA) center on the use of clustered optical and radio diagnostics in the Peruvian sector to address unresolved problems in equatorial aeronomy. The MISETA campaign conducted in September 1998 offered the first opportunity to test the wind suppression mechanism using a new Fabry-Perot interferometer (FPI) observing strategy in conjunction with new Global Positioning System (GPS) characterizations of ESF. As shown in subsequent sections, a relatively short observational campaign produced a rather clear set of conclusions on the ESF variability issue.

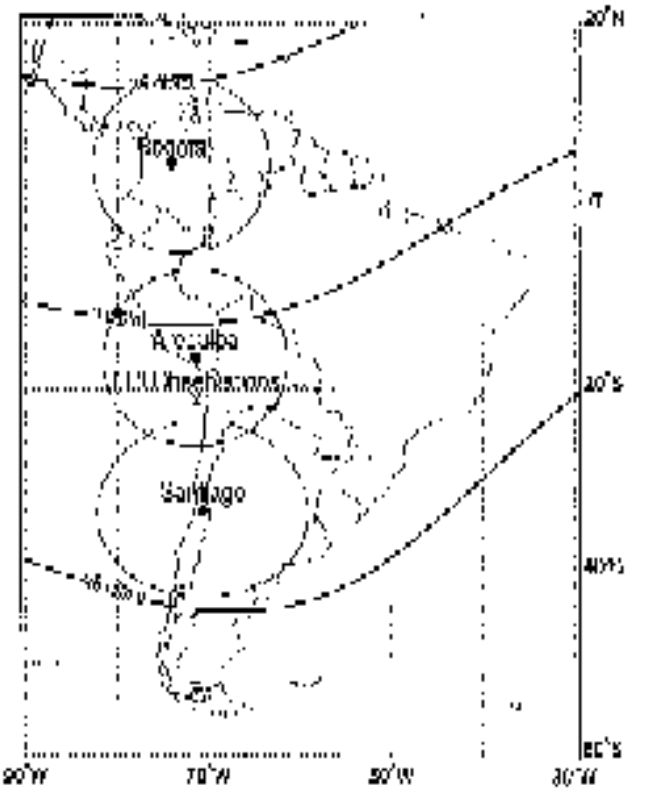

Figure 1. The Fabry-Perot interferometer (FPI) and GPS observing sites used in the Multi-Instrumented Studies of Equatorial Thermospheric Aeronomy (MISETA) campaign of September 1998. The station locations are indicated by the dots, while the circles give the fields of view for GPS observations at elevation angles above 15° for the three sites. At Arequipa, the large cross indicates where the FPI made high time resolution wind observations in the 6300-nm airglow layer; the circle also corresponds to the field of view of the all-sky images at that site.

2. Observations

Figure 1 shows the locations of the FPI and GPS sites (and their fields of view) in geographic and geomagnetic coordinates. The Arequipa FPI and its role in MISETA studies have been described by *Colerico et al*. [1996], *Meriwether et al*. [1997], and *Biondi et al*. [1999]. For the MISETA 1998 campaign, the regular five-position (N-S-E-W-Z) observing routine was changed to focus mainly on the southern position (at an elevation angle of 30°) to increase the frequency of measurements of the meridional wind component. The strategy adopted was to observe the meridional wind component in the south for ~75% of the total observing time. Added to this set of data points were occasional zenith measurements (~15%) required for the determination of the Doppler zero needed to calculate Doppler shifts, and zonal measurements (10%) were inserted to assess any unusual aspects of the thermosphere's horizontal flow on the nights in question. For each data point the acquisition of FPI spectral scans, each lasting 1 min, was continued until sufficient signal was accumulated to achieve a Doppler shift accuracy of ±15–20 m/s. Modeling studies of the centroid

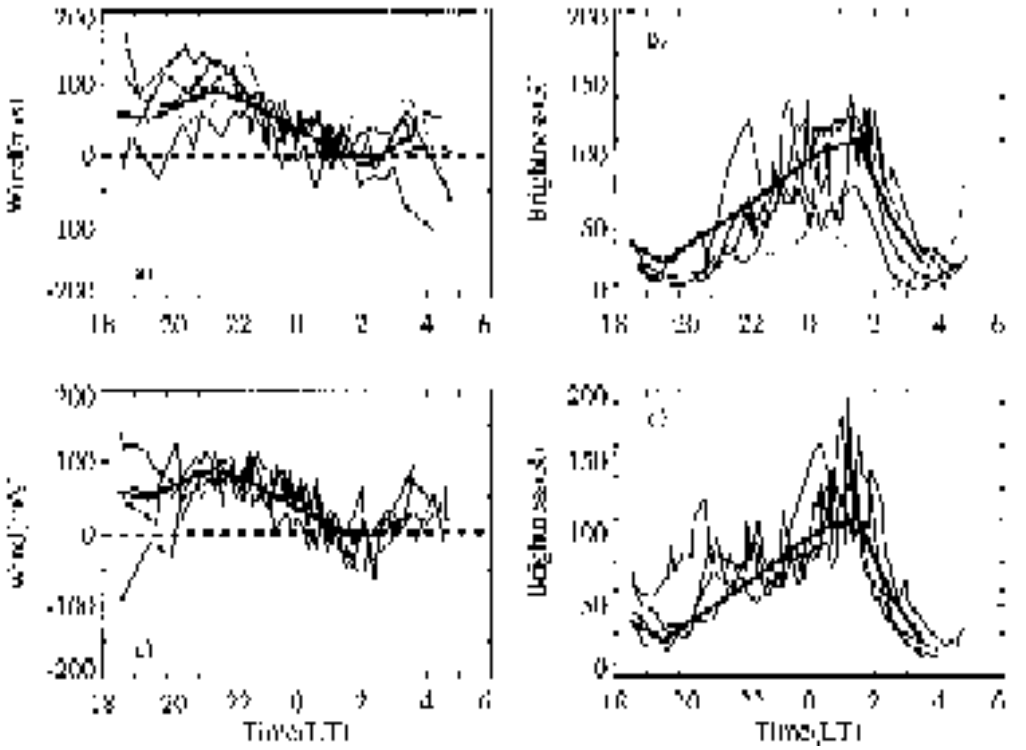

Figure 2. FPI determinations of thermospheric meridional winds and 6300-Å brightness levels during nine nights of the MISETA campaign of September 1998. Positive winds are northward, i.e., toward the equator from Arequipa. The thin lines show the nightly behavior on four nights of strong equatorial spread *F* (ESF) activity (Figures 2a and 2b) and four nights of weak ESF activity (Figures 2c and 2d). The dotted lines in Figures 2a and 2b give results on a night of high geomagnetic activity. The bold solid lines give the overall averages for the eight geomagnetically quiet nights. See also Table 1.

height of the 6300-Å airglow layer conducted by *Meriwether et al*. [1997] show that for the local times and solar flux levels of relevance here, the FPI observes winds in the 250- to 300-km height range. Thus wind variability effects at dusk cannot be due to the FPI observing dynamics at widely separated heights.

The determination of the meridional wind component can be made by observations to either the north or the south. We chose the southern direction because the higher electron densities of the southern Appleton anomaly located south of Arequipa increase the 6300-Å airglow brightness observed at 30° elevation by 20–30% over that seen in the north. This is consistent with the observed latitude gradient in the *F* region total electron content (TEC) to be shown below. The goal of the campaign was to get the first-ever set of high-time-resolution equatorial meridional winds in the early postsunset hours, and that was achieved at the loss of extensive companion data for the other directions. We emphasize that to test the physics embodied in (1), wind measurement throughout the dusk period are needed, and thus pushing the FPI technique to as close to sunset as possible represents state-of-the-art capabilities.

The three circles in Figure 1 give the GPS fields of view for receivers in Bogota, Arequipa, and Santiago. The GPS data yield two ionospheric *F* region parameters: the equivalent vertical total electron content (TEC) along the common meridian of ~70°W, and the GPS signal phase fluctuations used to document the presence of ionospheric irregularities associated with ESF. Both of these derived parameters involve assumptions that are standard in the field: a TEC "shell height" at 400 km and the rejection of noise spikes in the phase data. The specifics of GPS data processing methods developed to extract the latitudinal profiles of TEC versus local time and the quantitative portrayal of phase fluctuations are treated in detail by *Mendillo et al*. [2000]. *Aarons et al*. [1996] have demonstrated the reliability of using GPS phase fluctuation parameters to characterize ESF by making comparisons with well-known optical and radar methods, and *Beach and Kintner* [1999] have modeled the GPS sensitivity to plasma irregularity scale sizes within ESF events.

The MISETA 1998 FPI/ESF campaign was conducted from September 18 to 30, 1998. Of 13 nights of observations, only three nights of FPI data were lost due to cloud cover (GPS observations were available continuously). The results of these meridional wind measurements appear in Figure 2. The data sets have been divided into two groups based upon ESF activity. In Figures 2a and 2b, meridional winds and 6300-Å brightness levels observed on four nights of high ESF are shown by the thin lines. The dotted lines give results for September 25, a night of high geomagnetic activity (data for the second night of this storm period are not shown). In Figures 2c and 2d, similar measurements on four nights of low ESF activity are shown. The bold solid lines in all four panels of Figure 2 represent the means of the hourly averages for all eight of the geomagnetically quiet nights and give some indication of the climatological patterns of the meridional winds and the 6300-Å brightness levels. These wind averages are consistent with the long-standing morphology for meridional winds determined at this site for equinox, low solar flux periods [*Biondi et al*., 1991;

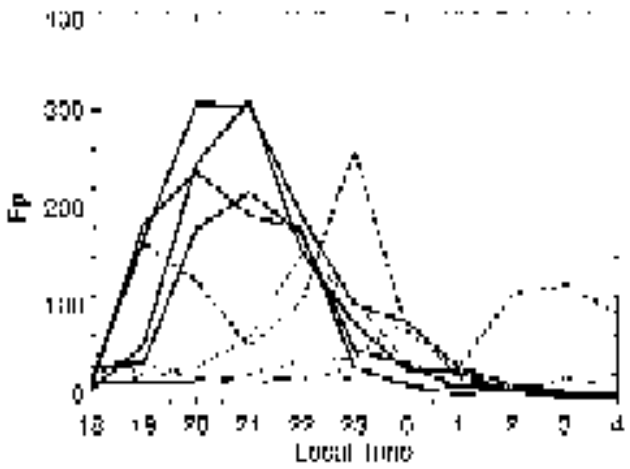

Figure 3. GPS-derived hourly values of phase fluctuation index (Fp) from the FPI site in Arequipa, Peru, during the same nine nights of neutral wind measurements shown in Figure 2. The bold lines indicate four nights of strong ESF activity and $\langle Kp \rangle = 3$; the thin lines indicate weak ESF activity and $\langle Kp \rangle = 2$; the dashed line describes a geomagnetic storm night, $\langle Kp \rangle = 8$, with bursts of ESF.

Biondi et al., 1999]. Further, our success in obtaining early evening (1830–2000 LT) measurements revealed more night-to-night variability than is observed near local midnight, thereby offering encouragement that the early evening data set is appropriate for correlation studies with GPS-derived ESF indicators.

In Figure 3 we present the hourly indices of GPS phase fluctuations for the same nine nights shown in Figure 2. As described by *Mendillo et al*. [2000], the Fp index for Arequipa GPS data reaches values ≥200 on nights of very strong ESF. This occurred during the sunset-to-midnight hours on four of the nine nights in the present study, as shown by the four bold lines in Figure 3. On four other nights where very little or weak ESF occurred, low values of Fp were noted, as indicated by the thin solid lines. On the one night of strong geomagnetic activity (September 25), bursts of ESF occurred in the postsunset, midnight, and predawn periods, with corresponding Fp values indicated by the bold dashed line. Excluding this unusual night, we are left with an excellent data set of four strong ESF nights and four weak ESF nights to compare with the corresponding meridional thermospheric wind variability.

3. Results

In Table 1 we summarize the full set of FPI, GPS, and geomagnetic conditions to be discussed. In the first column, the campaign date (in universal time) is given; the nightly FPI winds at dusk (average between 2300 and 0000 UT, the last hour of the previous UT date, corresponding to 1800 and 1900 LT) appear in the second column (with positive winds northward, the usual direction for this time and season). In the third and fourth columns the maximum GPS Fp indices during the premidnight period are given for both Arequipa and Bogota. As explained by *Mendillo et al*. [2000], Arequipa GPS phase fluctuation data pertain to near-equatorial (geomagnetic) regions where electron density irregularities in the bottomside F region do not necessarily imply the full development of high-altitude ESF plumes. The Fp values at Bogota remove this potential ambiguity. A high Fp at this northern equatorial anomaly site confirms ESF phenomena spanning flux tubes that extend to at least 1000 km above the equator (to reach Bogota's field of view of 10–25°N dip latitude). Note that the four low-Kp nights of greatest Fp at Arequipa (September 18, 22, 24, and 29) coincide with the same behavior at Bogota. This confirms our characterization of strong ESF nights for these dates. Similarly, the four low-Kp nights of non-ESF plumes are September 19, 20, 23, and 30 at both sites. The September 23, 1998, case is a good example of some bottomside structuring confined to Arequipa's location.

The two columns labeled "anomaly indicators" represent ways to use GPS-derived TEC versus latitude patterns to estimate thermospheric and electrodynamical processes operating in the postsunset equatorial ionosphere. Figure 4 shows the nine nights of TEC data obtained from the Bogota-Arequipa-Santiago chain obtained shortly after dusk. The equatorial ionization anomaly (EIA) is clearly evident on each night, with considerable variability in structure. *Mendillo et al*. [2000] defined two indices to characterize the EIA from such data: (1) I_s, an index to portray the mean peak-to-trough strength of the anomaly ($I_s = (N + S)/2M$), and (2) I_a, an index to portray the north versus south crest differences, or asymmetry of the

Table 1. Parameters Used in the MISETA Equatorial Spread F (ESF) Variability Study, September 1998[a]

		ESF Indicators		Anomaly Indicators		Magnetic Activity	
Date, UT	Winds: FPI $\langle U \rangle$ (Meridional) (m/s) 2300–0000 UT (1800–1900 LT)	GPS (Fp) max Arequipa 0000–0500 UT (1900–2400 LT)	GPS (Fp) max Bogata 0000–0500 UT (1900–2400 LT)	GPS/TEC I_s Anomaly Strength 0030 UT (1930 LT)	GPS I_a Anomaly Asymmetry 0030 UT (1930 LT)	Kp, 0000–0300 UT (1900–2200 LT)	Dst (max), 0000–0300 UT (1900–2200 LT)
18	−27	211	385	2.0	.5	2+	−8
19	12	34	36	1.8	.4	3	−47
20	−117	48	33	2.0	.5	3	−40
22	121	360	174	4.4	.7	0	−30
23	41	175	69	1.9	.3	3	−35
24	71	237	676	3.9	.7	3+	−47
25	119	319	81	2.2	.3	8−	−93
29	−6	313	421	5.8	.1	1	−36
30	84	34	35	1.4	.2	2	−30

[a]Days of highest ESF are September 18, 22, 24, and 29. Days of lowest or no ESF are September 19, 20, 23, and 30. Day of high geomagnetic activity is September 25. Campaign day is specified for the 0000–0500 UT period, and thus LT periods (1900–2400 LT) refer to previous day.

anomaly ($I_a = [(N - S)/(N + S)/2]$), where N, S, and M are the north, south, and intervening minimum values, respectively. To interpret these indices physically, we associate high I_s values with strong electrodynamical uplift that leads to a more dramatic Appleton anomaly. Strong $\mathbf{E} \times \mathbf{B}$ vertical drifts enhance ESF growth rates, and thus I_s and Fp should be positively correlated, all other things being equal. Conversely, the I_a index should be associated with enhanced meridional winds that would distort a presumed symmetrical anomaly, a proposed inhibitor of ESF growth rates. Thus stronger meridional winds ($|U_m|$) should be positively correlated with I_a, and both U_m and I_a should be anticorrelated with Fp.

A graphical representation of these correlation attempts appears in Figure 5. In Figure 5a the mean Fp results for Arequipa and Bogota show that ESF activity differed by a factor of 7 between the high ESF and low ESF four-day sample sets. In Figure 5b the absolute values of the meridional winds at dusk have nearly the same mean values in both four-night groups, providing no evidence that neutral meridional winds affect either ESF onset or suppression.

The Appleton anomaly asymmetry index (I_a) analysis reveals some unanticipated results. The mean winds (Figure 2) are northward in the dusk sector, consistent with a TEC asymmetry favoring the northern crest (as shown in Figure 4). Yet in Table 1, the day-to-day variations in the magnitude and direction of the winds at dusk do not correlate with the I_a variations. In Figure 5c the mean asymmetry values for the high versus low ESF nights are statistically equivalent, as are the meridional winds for both four-night samples (Figure 5b). Taken together, Figures 5a–5c provide little evidence for wind-induced asymmetries being a consideration for ESF onset.

Figure 5d shows a factor of 2 difference between I_s values on high- and low-ESF nights. An examination of the individual values in Table 1 reveals complete consistency between the four nights of low I_s and low Fp and a clear three out of four

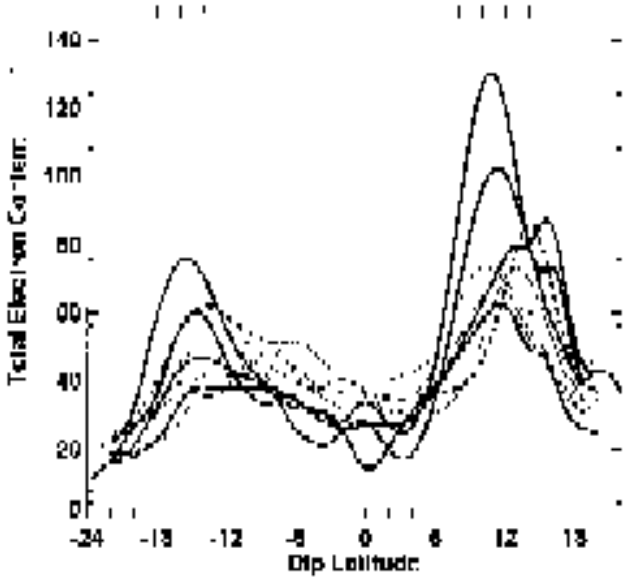

Figure 4. GPS-derived total election content (TEC) plotted against geomagnetic dip latitude at 0030 UT (corresponding to 1930 LT) for the nine nights of observations. As in Figure 3, bold lines indicate nights of strong ESF, light lines indicate weak ESF, and the dashed line indicates a geomagnetic storm night.

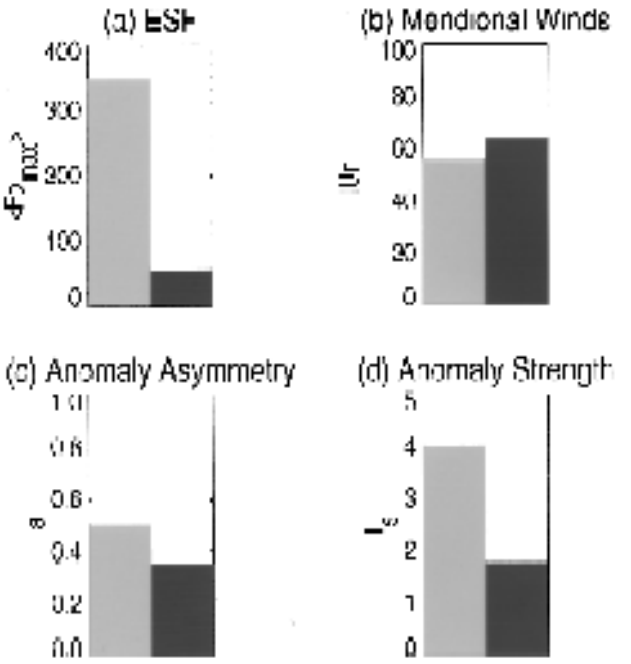

Figure 5. Comparisons of various averaged quantities for the four strong ESF nights (lighter shaded boxes) and the four weak/no-ESF nights (darker shaded boxes) as given in Table 1. $\langle Fp \rangle$ max is the mean of the Arequipa and Bogota GPS maximum phase fluctuations indices from 2000 to 2400 LT; U_m is the average measured meridional winds (in m/s) around 1830 LT (2330 UT); and I_s and I_a are the Appleton anomaly strength and asymmetry indices, respectively, at 1930 LT.

pattern for the strong Fp nights. This suggests, once again, that the only successful precursor for ESF onset is an ionosphere dominated by electrodynamical activity near dusk [*Fejer et al.*, 1999, and references therein]. The early evening 6300-Å airglow brightness patterns shown in Figures 2b and 2d offer additional evidence for the dominance of vertical drifts on nights of high ESF. The low airglow values around 1830–2000 LT in Figure 2b result from reduced dissociative recombination, an effect long known to occur on nights when the upward plasma drift moves the F region peak plasma to high altitudes ($\geq$400 km), inhibiting the formation of the molecular ions (O_2^+) that upon dissociative recombination produce 6300-Å emission. This trend does not occur on the non-ESF nights shown in Figure 2d.

The MISETA all-sky imager, colocated with the FPI in Arequipa, provides the broad spatial and dynamical contexts for 6300-Å structures at low latitudes [*Mendillo et al.*, 1997]. As illustrated in Figure 1, the geomagnetic equator spans the upper third of the field of view. This geometry results in geomagnetic flux tubes crossing the equator that have apex heights near the F region peak and not at great topside heights that would have conjugate regions near Bogota and Santiago.

Figure 6 contains examples of imaging data taken on seven of the nine nights described in Table 1 and in earlier figures. The imager operates fewer nights per month than the FPI in order to avoid having the bright Moon overwhelm the low light level airglow. Thus no images were taken on the clear nights of September 29 and 30. In the top row of Figure 6, three nights of strong ESF show classic 630-nm airglow depletions: the dark north-south bands marking the feet of geomagnetic flux tubes

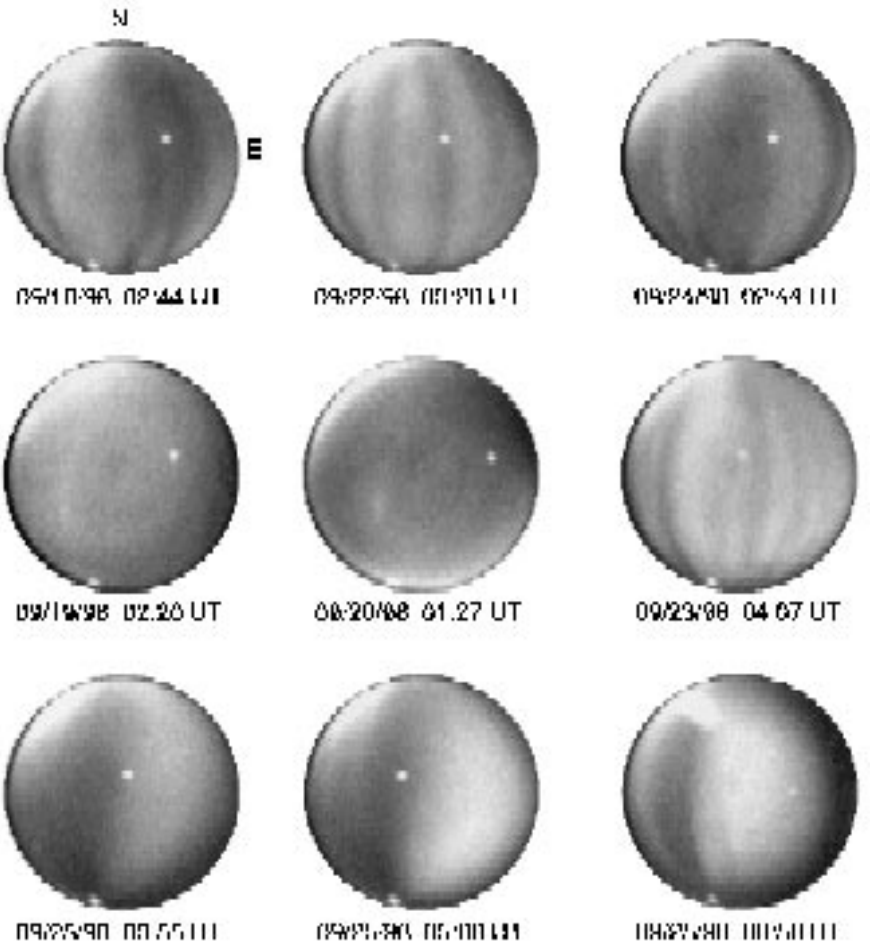

Figure 6. Examples of 6300-Å all-sky images taken in Arequipa on seven of the nine nights used in this study (see text). The persistent bright region to the northwest comes from the city lights of Arequipa, and the small bright "dot" near the center of each image is the appearance of Jupiter through the 6300-Å filter. Times are in universal time to be consistent with dates in Table 1; LT equals UT minus 5 hours.

with low-electron densities in the airglow generating regions near 300 km. In the middle row of Figure 6 the left two samples show unstructured airglow on the no-ESF nights of September 19 and 20. The third case in the middle row shows the interesting case of airglow depletions on a night of weak ESF (September 23). The pattern is similar in appearance to those in the top row, pointing out that an image at Arequipa's location is incapable of distinguishing ESF events that are geomagnetically localized (in height and latitude) from fully developed interhemispheric (topside) ESF plumes. This is precisely why we chose to use the multisite GPS phase fluctuation method of defining ESF events. If only Arequipa-based instruments had been used on this night, its GPS value of $F_p = 175$ and its images in the middle row of Figure 6 might have suggested a robust EFS event. The F_p values at Bogota and Santiago (69 and 25, respectively), however, clearly identify September 23 to be a night of bland, equatorially confined irregularities, as shown in the model results of *Seker and Kelley* [1998].

The bottom row in Figure 6 gives three examples of airglow depletions throughout the geomagnetically disturbed night of September 25. The depletions are different in character from those shown in the top row; for example, they are far more broad in longitudinal width. This reinforces the decision to exclude storm-time ESF periods from our study of day-to-day variability.

4. Prediction of ESF Events

The U.S. component of the international space physics community has embarked on a major reorientation of the reasons for studying solar-terrestrial physics, namely, the desire to predict disruptions in the space environment that might affect technological systems. In the aeronomic domain, perhaps the most serious potential "space weather" phenomena arise from ESF effects upon radio communication systems. This points out a most unusual aspect of this new paradigm, namely, that the single most disruptive effect upon radio propagation in the upper atmosphere (ESF) is not related directly to the solar, solar wind, and magnetospheric-coupling drivers that are the major foci of space weather research. Nevertheless, a disruptive, variable component of the upper atmospheric system, whether triggered internally or externally, is still in need of forecasting. Yet within this context of an increased attention to predicting ESF, there has been little thoughtful discussion of the actual practicality of such efforts. Given the known longitude pattern for "ESF seasons," the problem of prediction

reduces to two classes of events: (1) the day-to-day variability within ESF season at a given longitude, and (2) the instigation or inhibition of ESF during periods of geomagnetic activity, regardless of season. Moreover, both categories show differences in ESF occurrence during the postsunset and postmidnight local time periods.

Space weather research today finds itself somewhere between the extremes of describing a fully deterministic system versus coping with the practical reality of seemingly chaotic subsystems. No example typifies this better than equatorial spread F. ESF events are highly localized in space and time, and thus attempting an actual prediction is essentially equivalent to the meteorological task of predicting the time when a specific neighborhood will be struck by a tornado. It is unlikely that tropospheric scientists would propose to accomplish this with lead times of several hours to a full day. Space scientists and government program managers should not propose the equivalent as attainable space weather goals. So-called "now-casting" and tracking of a detected ESF disturbance are far more achievable goals. Yet it is scientifically abhorrent to abandon the search for cause-effect relationships.

A possible intermediate goal between these extreme views is the concept of using ionospheric-thermospheric parameters "near sunset" (as variously defined) to enable a short-term prediction of ESF after sunset. Several studies have dealt with this problem, as will be discussed below. First, it is important to realize that predicting a specific strength level of ESF to occur within a narrow time bin (e.g., 2200–2300 LT) from measurements in an earlier time bin (say, 1800–1900 LT) has never been attempted, nor is it likely to succeed. Studies to date have dealt with using dusk sector observations to predict whether or not ESF will occur sometime during the following 6–12 hours, as done in the present study. In such cases, there is no attempt to discriminate between ESF forming over the site in question versus that site experiencing an ESF disturbance drifting into its field of view.

The first success achieved in finding ESF precursors was in the work of *Raghavarao et al*. [1988] using ionosonde data from three stations near and northward of the geomagnetic equator in India. They found that an intensification in the trough-to-crest gradient of the equatorial ionization anomaly (EIA) in the 270- to 300-km altitude range between 1700 and 1900 LT occurred prior to ESF occurrence the same night. *Sridharan et al*. [1994] realized that EIA latitude gradient effects in bottomside electron densities would coincide with 6300-Å airglow layer signatures. They demonstrated that new dayglow instrumentation from a single site, approximately midway between the EIA trough and crest in India, could sense the same effect as early as 1600 LT, thus providing a prediction of ESF at least 3 hours prior to its actual occurrence.

Given that the ionosphere has strong longitude effects, and particularly so with ESF patterns, it is reasonable to ask if a predictive scheme formulated and tested in one sector would work in another. Accordingly, *Alex et al*. [1989] used three ionosonde stations in the American longitude sector that spanned the EIA from its trough to its northern crest; they reported that steep electron density gradients at fixed bottomside heights indeed occurred prior to postsunset ESF.

In the only satellite-based prediction method developed and tested to date, *Sultan* [1996a, 1998] used in situ plasma density measurements at the altitude of the DMSP satellites (840 km) to characterize transequatorial gradient patterns of the EIA and their relationship to the subsequent development of ESF. The results were most promising and represent the first approach to the problem that might actually have operational potential for specification and forecast.

In each of the studies mentioned above, the gradient effects noted were attributed to dynamical processes induced by strong electrodynamics, either directly or via neutral wind induced motions. That is, a stronger EIA was a good indicator for ESF to develop regardless of the specific mechanism proposed. On the other hand, *Fagundes et al*. [1999] used a variety of optical and radio sounding observations to show that a complex blend of gradients, seeds, and drifts determined what a site experienced on a given night. While not a prediction paper per se, Fagundes et al. essentially argue that no single parameter could be used to forecast ESF. Finally, *McClure et al*. [1998] used a comprehensive analysis of the longitude-seasonal occurrence patterns for ESF to propose that gravity wave seeding is the dominant factor in ESF variability. Again, while not a day-to-day prediction paper per se, McClure et al. certainly imply that given favorable background conditions, the availability or lack of gravity waves determines if ESF occurs on a given night.

In this study we used the full interhemispheric pattern of the EIA to characterize the day-to-day variations between crests and trough in TEC, and their relationship to subsequent phase fluctuations, using three simple indices (I_s, I_a, Fp). Given the flux-tube-integrated nature of the physics driving the instability, use of TEC might offer a better way to describe such effects, rather than single height gradients in electron density. Indeed, if bottomside gradient effects show promise in one hemisphere (as in the work of *Raghavarao et al*. [1988], *Alex et al*. [1989], and *Sridharan et al*. [1994]), and topside signatures at the DMSP altitude point to useful forecasts (as shown by *Sultan* [1996b, 1998]), then integrated electron density altitude profiles available from GPS networks at low latitudes might be expected to be both a favorable now-casting tool and a potential predictor of ESF. Having both the forecast parameter (I_s) and the detection of the predicted effect (Fp) available from the same instruments at the same sites offers obvious advantages. It remains to be seen, however, if the limited case-study trend depicted in Figures 5a and 5d, linking ESF to a quantitative measure of the EIA strength, could be a reliable forecast scheme at all longitudes and epochs of solar activity (as discussed in more detail by *Mendillo et al*. [2000]).

5. Summary and Conclusions

A multidiagnostic observing campaign conducted via the MISETA consortium was formulated to test a hypothesis concerning the day-to-day control of equatorial spread F. The proposal that strong thermospheric winds flowing across the geomagnetic equator could inhibit or suppress ESF onset had been advanced to explain seasonal-longitude patterns by *Maruyama and Matuura* [1984] and, potentially, day-to-day variability [*Mendillo et al*., 1992]. Additional simulation studies by *Zalesak and Huba* [1991] and *Kuo et al*. [1998] reinforced the role of thermospheric dynamics on the instability growth rate as described in earlier studies [*Zalesak et al*., 1982; *Maruyama*, 1988]. Yet little experimental effort was devoted to this topic in the many years following its proposal. This was due, in part, to the limited diagnostics for measuring thermospheric winds in the dusk/sunset sector, as well as to the need for a consistent quantitative way to characterize ESF activity along transequatorial flux tubes.

In the present study we have improved on the previously sparse observations of meridional winds in the dusk sector by sacrificing full wind vector measurements in favor of higher time resolution of the meridional wind component. Also, the recent availability of low-latitude GPS diagnostics for ionospheric structure and irregularities has provided the continuous spatial and temporal coverage needed for accurate specification of ESF occurrence. The resulting MISETA 1998 campaign for studies of meridional wind behavior and ESF occurrence has produced eight nights of excellent data, admittedly a small data set for geophysical research. Yet the trend revealed is unambiguous; that is, no convincing evidence has been found that meridional winds at dusk exert a strong influence on ESF onset in the subsequent premidnight hours.

On seven of the eight nights the only reliable predictor of ESF onset is the strength (peak-to-trough ratio) of the Appleton anomaly in GPS-derived TEC versus latitude at dusk. This ratio is governed primarily by the electrodynamical vertical drift near sunset. Thus the initial suggestion for ESF onset control by the zonal electric field made by *Booker and Wells* [1938] and later reinforced by *Farley et al*. [1970] and in every decade since [*Abdu et al*., 1983; *Sastri*, 1984; *Kelley and Maruyama*, 1992; *Jayachandran et al*., 1993; *Sultan*, 1996a; *Fejer et al*., 1999] remains the dominant answer to the question of day-to-day variability in ESF occurrence. The complete lack of evidence that variable meridional winds govern the asymmetry in the EIA crest magnitudes in day-to-day TEC observations is an area in need of more model studies.

The dominant role exerted by vertical plasma drift upon day-to-day ESF occurrence has been addressed in recent simulation studies. *Seker and Kelley* [1998, and references therein] presented modeling scenarios that varied the strength and duration of the postreversal enhancement in vertical drift to see the consequence on subsequent Rayleigh-Taylor instability development. While they pointed out that it is difficult at present to set specific values to the magnitudes and durations of the drifts that lead to ESF, they did conclude (p. 20,745) that "the condition of small or little prereversal enhancement provides a favorable situation for the confinement of the irregularities in the bottomside of the ionosphere."

Finally, in the current era of renewed interest in forecasting ionospheric disruptions on radio communications, the interesting question is, How successful does a forecast have to be? From our limited sample of eight geomagnetically quiet nights listed in Table 1, seven successful forecasts (85%) of strong ESF occurrence would have been achieved by using an anomaly strength (I_s) criterion of $I_s \geq 4$. This GPS-derived proxy for electrodynamic vertical drift may turn out to be site and season dependent in its quantitative use, but at present this approach looks promising. Surely, it is more successful than predicting ESF suppressions through measurements of meridional wind speeds. For the only night of its failure (September 18, with $I_s = 2$), conventional wisdom offers three possibilities: (1) strong meridional winds (contrary to observations in Table 1), (2) no seed perturbation (e.g., gravity wave), or (3) an enhanced nighttime E region layer of ionization that suppresses F region electrodynamics [*Tsunoda*, 1985]. That the variability of seeds controls ESF has been discussed recently by *McClure et al*. [1998]; a modeling examination of the suppression of ESF due to the occurrence of a low latitude sporadic E layer was presented by *Stephan et al*. [1997]. In view of the inherent variability of the geophysical system, predictive attempts for ESF may well be achievable only to the 85% success level (at best). The pursuit of additional parameters capable of being measured in real time at many longitudes (gravity waves and sporadic E layers), but difficult to assess quickly for quantitative prediction schemes, might not be a productive to way deal with a potentially acceptable one out of eight failure rate.

Acknowledgments. Funding support for this research was provided by the National Science Foundation CEDAR and NSF Aeronomy programs through grant awards ATM-9714771, ATM-9714770, and ATM-9414403 to M. Mendillo, J. Meriwether, and M. Biondi, respectively. Space and on-site technical support for the operations of the FPI instrument at the NASA Satellite Laser Ranging Station at Arequipa, Peru, are provided by the National Aeronautics and Space Administration. The GPS data used in the study were obtained from the International GPS Service (IGS) from Geodynamics, http://igscb.jpl-.nasa.gov. The analysis of GPS data at Boston University is supported by grants from the Office of Naval Research (N00014-89-5-1754) and NASA (NAG5-4707).

Janet G. Luhmann thanks the referees for their assistance in evaluating this paper.

References

Aarons, J., The longitudinal morphology of equatorial F layer irregularities relevant to their occurrence, *Space Sci. Rev*., *63*, 209–243, 1993.

Aarons, J., M. Mendillo, R. Yantosca, and E. Kudeki, GPS phase fluctuations in the equatorial region during the MISETA 1994 campaign, *J. Geophys. Res*., *101*, 26,851–26,862, 1996.

Abdu, M. A., R. T. de Medeiros, J. A. Bittencourt, and I. S. Batista, Vertical ionization drift velocities and range type spread F in the evening equatorial ionosphere, *J. Geophys. Res*., *88*, 399–402, 1983.

Alex, S., P. V. Koparkar, and R. G. Rastogi, Spread-F and ionization anomaly belt, *J. Atmos. Terr. Phys*., *51*, 371–374, 1989.

Beach, T. L., and P. M. Kintner, Simultaneous Global Positioning System observations of equatorial scintillations and total electron content fluctuations, *J. Geophys. Res*., *104*, 22,553–22,565, 1999.

Biondi, M. A., J. W. Meriwether Jr., B. G. Fejer, S. A. Gonzalez, and D. C. Hallenbeck, Equatorial thermospheric wind changes during the solar cycle: Measurements at Arequipa, Peru, from 1983 to 1990, *J. Geophys. Res*., *96*, 15,917–15,931, 1991. (Correction, *J. Geophys. Res*., *100*, 7863, 1995.)

Biondi, M. A., S. Y. Sazykin, B. G. Fejer, J. W. Meriwether, and C. G. Fesen, Equatorial and low-latitude thermospheric winds: Measured quiet time variations with season and solar flux from 1980 to 1990, *J. Geophys. Res*., *104*, 17,091–17,106, 1999.

Booker, H., and H. W. Wells, Scattering of radio waves by the F region of the ionosphere, *J. Geophys. Res*., *43*, 249–256, 1938.

Colerico, M., M. Mendillo, D. Nottingham, J. Baumgardner, J. Meriwether, J. Mirick, B. Reinish, J. Scali, C. Fesen, and M. A. Biondi, Coordinated measurements of F region dynamics related to the thermospheric midnight temperature maximum, *J. Geophys. Res*., *101*, 26,783–26,793, 1996.

Fagundes, P. R., Y. Sahai, I. S. Batista, M. A. Abdu, J. A. Bittencourt, and H. Takahashi, Observations of day-to-day variability in precursor signatures to equatorial F region plasma depletions, *Ann. Geophys*., *17*, 1053–1063, 1999.

Farley, D. T., B. B. Balsley, R. F. Woodman, and J. P. McClure, Equatorial spread F: Implications of VHF radar observations, *J. Geophys. Res*., *75*, 7199–7216, 1970.

Fejer, B. G., Low latitude electrodynamic plasma drifts: A review, *J. Atmos. Sol. Terr. Phys*., *53*, 665–675, 1991.

Fejer, B. G., The electrodynamics of the low-latitude ionosphere: Recent results and future challenges, *J. Atmos. Sol. Terr. Phys*., *59*, 1456–1482, 1997.

Fejer, B. G., L. Scherliess, and E. R. de Paula, Effects of the vertical plasma drift velocity on the generation and evolution of equatorial spread F, *J. Geophys. Res*., *104*, 19,859–19,869, 1999.

Fuller-Rowell, M., V. Codrescu, B. G. Fejer, W. Borer, F. Marcos, and D. N. Anderson, Dynamics of the low-latitude thermosphere: Quiet and disturbed conditions, *J. Atmos. Sol. Terr. Phys*., *59*, 1533–1540, 1997.

Haerendel, G., Theory of equatorial spread F, report, Max Planck Inst. for Extraterr. Phys., Garching, Germany, 1973.

Haerendel, G., J. V. Eccles, and S. Cakir, Theory for modeling the equatorial evening ionosphere and the origin of the shear in the horizontal plasma flow, *J. Geophys. Res*., *97*, 1209–1223, 1992.

Huang, C. S., and M. C. Kelley, Nonlinear evolution of equatorial spread *F*, 2, Gravity wave seeding of Rayleigh-Taylor instability, *J. Geophys. Res*., *101*, 293–302, 1996.

Huba, J. D., P. A. Bernhardt, S. L. Ossakow, and S. T. Zalesak, The Rayleigh-Taylor instability is not damped by recombination in the *F* region, *J. Geophys. Res*., *101*, 24,553–24,556, 1996.

Hysell, D. L., M. C. Kelley, W. E. Swartz, and R. F. Woodman, Seeding and layering of equatorial spread *F* by gravity waves, *J. Geophys. Res*., *95*, 17,253–17,260, 1990.

Jayachandran, B., N. Balan, P. B. Rao, J. H. Sastri, and G. J. Bailey, HF Doppler and ionosonde observations on the onset conditions of equatorial spread *F*, *J. Geophys. Res*., *98*, 13,741–13,750, 1993.

Kelley, M. C., *The Earth's Ionosphere*, *Int. Geophys. Ser*., vol. 43, Academic, San Diego, Calif., 1989.

Kelley, M. C., and T. Maruyama, A diagnostic model for equatorial spread *F*, 2, The effect of magnetic activity, *J. Geophys. Res*., *97*, 1271–1277, 1992.

Keskinen, M. J., S. L. Ossakow, S. Basu, and P. J. Sultan, Magnetic-flux-tube-integrated evolution of equatorial ionospheric plasma bubbles, *J. Geophys. Res*., *103*, 3957–3967, 1998.

Kuo, F. S., S. Y. Chou, and S. J. Shau, Comparison of topside and bottomside irregularities in equatorial *F* region ionosphere, *J. Geophys. Res*., *103*, 2193–2199, 1998.

Maruyama, T., A diagnostic model for equatorial spread *F*, 1, Model description and application to electric field and neutral wind effects, *J. Geophys. Res*., *93*, 14,611–14,622, 1988.

Maruyama, T., and N. Matuura, Longitudinal variability of annual changes in activity of equatorial spread *F* and plasma bubbles, *J. Geophys. Res*., *89*, 10,903–10,912, 1984.

McClure, J. P., S. Singh, D. K. Bamgboye, F. S. Johnson, and H. Kil, Occurrence of equatorial *F* region irregularities: Evidence for tropospheric seeding, *J. Geophys. Res*., *103*, 29,119–29,135, 1998.

Mendillo, M., J. Baumgardner, X.-Q. Pi, P. J. Sultan, and R. T. Tsunoda, Onset conditions for equatorial spread *F*, *J. Geophys. Res*., *97*, 13,865–13,876, 1992.

Mendillo, M., J. Baumgardner, M. Colerico, and D. Nottingham, Imaging science contributions to equatorial aeronomy: Initial results from the MISETA program, *J. Atmos. Sol. Terr. Phys*., *59*, 1587–1600, 1997.

Mendillo, M., B. Lin, and J. Aarons, Applications of GPS observations to equatorial aeronomy, *Radio Sci*., *35*, 885–904, 2000.

Meriwether, J. W., M. A. Biondi, F. A. Herrero, C. G. Fesen, and D. C. Hallenbeck, Optical interferometric studies of the nighttime equatorial thermosphere: Enhanced temperatures and zonal wind gradients, *J. Geophys. Res*., *102*, 20,041–20,058, 1997.

Ossakow, S. L., Spread-*F* theories—A review, *J. Atmos. Sol. Terr. Phys*., *43*, 437–452, 1981.

Raghavarao, R., M. Nageswararao, J. Hanumath Sastri, G. D. Vyas, and M. Sriramarao, Role of equatorial ionization anomaly in the initiation of equatorial spread *F*, *J. Geophys. Res*., *93*, 5959–5964, 1988.

Sastri, J. H., Duration of equatorial spread *F*, *Ann. Geophys*., *2*, 353–358, 1984.

Seker, R., and M. C. Kelley, On the combined effects of vertical shear and zonal electric field patterns on nonlinear equatorial spread *F* evolution, *J. Geophys. Res*., *103*, 20,735–20,747, 1998.

Sridharan, R., D. Pallam Raju, R. Rahoavarao, and P. Ramarao, Precursor to equatorial spread-*F* in OI 630.0 nm dayglow, *Geophys. Res. Lett*., *21*, 2797–2800, 1994.

Stephan, A., M. Colerico, M. Fox, and M. Mendillo, Modeling of *E* region contributions to ionospheric instabilities (abstract), *Eos Trans. AGU*, *78*(46), Fall Meet. Suppl., F505, 1997.

Sultan, P. J., Linear theory and modeling of the Rayleigh-Taylor instability leading to the occurrence of equatorial spread *F*, *J. Geophys. Res*., *101*, 26,875–26,891, 1996a.

Sultan, P. J., Satellite signatures of the global occurrence morphology of equatorial spread *F*, in *Proceedings of the Ionospheric Effects Symposium (IES-96)*, edited by J. M. Goodman, pp. 287–292, Nav. Res. Lab., Washington, D. C., 1996b.

Sultan, P. J., DMSP observations of variability and irregularities in the low-latitude topside ionosphere (abstract), *Eos Trans. AGU*, *79*(17), Spring Meet. Suppl., S243, 1998.

Tsunoda, R. T., Control of the seasonal and longitudinal occurrence of equatorial scintillations by the longitudinal gradient in integrated *E* region Pederson conductivity, *J. Geophys. Res*., *90*, 447–456, 1985.

Zalesak, S. T., and J. D. Huba, Effect of meridional winds on the development of equatorial spread *F* (abstract), *Eos Trans. AGU*, *72*(17), Spring Meet. Suppl., 211, 1991.

Zalesak, S. T., S. L. Ossakow, and P. K. Chaturvedi, Nonlinear equatorial spread *F*: The effect of neutral wind and background Pedersen conductivity, *J. Geophys. Res*., *87*, 151–166, 1982.

M. Biondi, Department of Physics and Astronomy, University of Pittsburgh, Pittsburgh, PA 15620.

M. Mendillo, Center for Space Physics, Boston University, 725 Commonwealth Avenue, Boston, MA 02215. (mendillo@buasta.bu.edu)

J. Meriwether, Department of Physics and Astronomy, Clemson University, Clemson, SC 29634-0978.

(Received April 18, 2000; revised September 26, 2000;
accepted October 16, 2000.)